

Toward Controlling Folding in Synthetic Polymers: Fabricating and Characterizing Supramolecular Single-Chain Nanoparticles

Erik B. Berda, E. Johan Foster, and E. W. Meijer*

*Institute for Complex Molecular Systems and Laboratory of Macromolecular and Organic Chemistry,
Eindhoven University of Technology, P.O. Box 513, 5600 MB Eindhoven, The Netherlands*

Received October 28, 2009; Revised Manuscript Received December 28, 2009

ABSTRACT: We discuss in detail our facile method for producing supramolecular polymeric nanoparticles from the collapse of single polymer chains. A new family of poly(methyl methacrylate)-based nanoparticles confirm that our method is general and can be easily tuned toward a variety of applications. Thorough AFM characterization elucidates the conditions required to visualize single particles as well as complex assemblies of particles mediated by the evaporation of solvent. AFM studies also indicate that the intramolecular collapse resembles the cooperative folding process witnessed in biomacromolecules and that the particles possess a complex morphology that implies the internal organization of the UPy dimers used to induce the intramolecular collapse. Thermal studies support these observations in addition to confirming the applicability of this system in the fabrication of processable high-performance supramolecular materials.

Introduction

Vigorous research efforts persist in the area of polymeric nanoparticles. This is not surprising considering their applicability across the sciences from materials to medicine.^{1–14} Recently, a new method of producing polymer nanoparticles has become popular: the intramolecular cross-linking and collapse of single polymer chains.^{2,4,6–8,11,15–18} This method allows the facile preparation of nanoparticles from 5 to 20 nm in diameter with a wide variety of chemical compositions. The sizes of the particles made in this fashion are tunable simply by controlling the molecular weight of the parent polymer chain and the amount of cross-linking used to effect the collapse. In a sense, this work builds on previous work in foldamers¹⁹ by using a top-down approach to study folding in synthetic polymers, rather than the piecewise bottom-up approach used in foldamer synthesis.

In an attempt to advance the field of polymer nanoparticle synthesis toward the efficiency witnessed in nature, we have developed a method for producing well-defined polymeric nanoparticles using nature's design: single chains suspended in a metastable collapsed state by intramolecular, supramolecular cross-links.¹⁶ While our collapsed single-chain nanoparticles (SCNP) are by no means as structurally magnificent as folded biomacromolecules, they represent an advancement toward understanding the process of controlled polymer folding. The choice of polymer backbone composition for nature's SCNP construction is generally limited: phosphate ester linked ribose rings in nucleic acids or poly(amides) in proteins. In attempting to mimic this complex behavior synthetically, the choice of backbone architecture is daunting considering the virtually limitless possibilities. Given the ease in which exotic polymer structures can be made using ROMP,^{20–24} poly(norbornenes) (PNB) were a logical first choice for the backbone material of our SCNPs.¹⁶ We discuss here a new family of particles based on poly(methyl methacrylate) (PMMA) synthesized using a combination of living radical polymerization and "click" chemistry, providing a system that can be readily tuned. In doing so, we demonstrate that our method is general and can be applied to a wide array of

polymer and solvent systems, further expanding its utility. The methods used to fabricate and characterize this complex molecular system are discussed in greater depth, and we provide new insights as to their structure and behavior in the bulk when deposited on a surface. Our goal through continued development of this work is to create self-folding synthetic polymers which closely mimic, in both structure and function, nature's sophisticated nanomachinery.

Results and Discussion

Polymer Design. Our method, illustrated in Figure 1, involves the synthesis of a linear polymer chain functionalized with an *o*-nitrobenzyl-protected 2-ureidopyrimidinone (UPy) pendant moiety, linked to the polymer through a urethane or urea group. By diluting the polymer below the threshold concentration (c^*) and irradiating with UV light, we induce the intramolecular collapse via supramolecular interactions. We chose to work with PMMA in this report of a number of reasons: living radical polymerization techniques such as ATRP^{25–33} and SET-LRP^{34–41} provide control over molecular weight and molecular weight distribution. As with ROMP, there is an enormous volume of work on the synthesis of functionalized PMMA-based materials, all of which could be potential SCNP candidates. While this is the case for many other monomers besides MMA, the propensity of PMMA to photodegrade gives us the opportunity to demonstrate the efficacy of the photodeprotection process. Finally, exchanging the PNB backbone for PMMA proves that increasing the polarity of the polymer backbone does not hinder the supramolecular collapse, opening this method to variety of possible functional polymer architectures.

Synthesis. Scheme 1 illustrates our initial synthesis of the PMMA SCNPs. Because of failed attempts to copolymerize the protected UPy–urethane comonomer **1** with MMA under normal ATRP conditions, we adopted the relatively new technique ARGET ATRP³² which is more active than traditional ATRP due to the constant regeneration of the active Cu(I) species. This route successfully provided protected UPy–urethane functionalized polymer **2** albeit with molecular

*Corresponding author. E-mail: e.w.meijer@tue.nl.

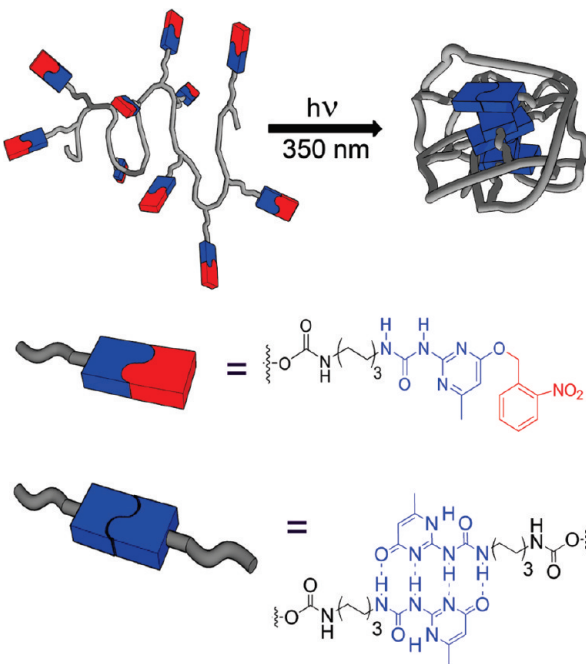
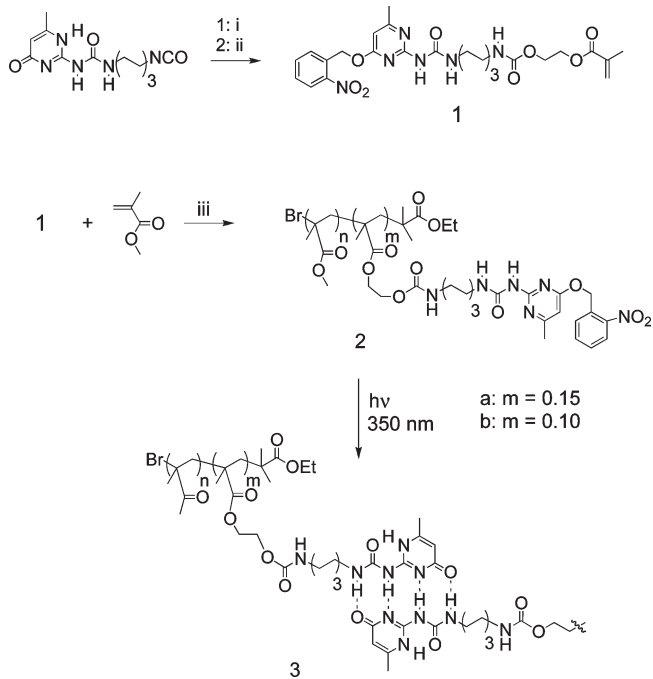


Figure 1. UV irradiation induced collapse of a single polymer chain into a nanoparticle via the supramolecular cross-linking of the UPy–urethane side groups (nitroaldehyde side product omitted for clarity).

Scheme 1. ARGET ATRP Synthesis of UPy–Urethane Functionalized PMMA^a

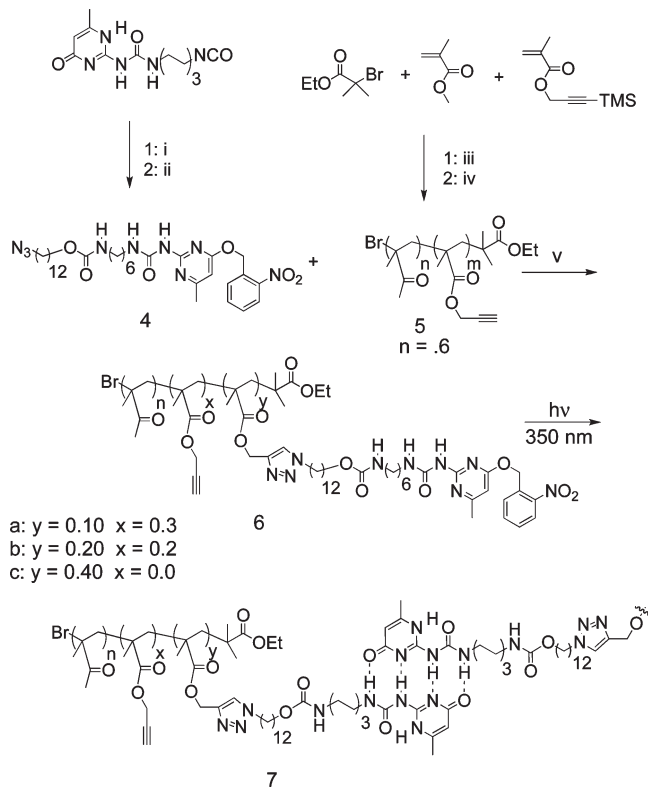


^a Reagents and conditions: (i) HEMA, DBDTL, CH_2Cl_2 ; (ii) *o*-nitrobenzyl chloride, K_2CO_3 , DMF; (iii) macroinitiator, PMDETA, CuBr , tin(II) 2-ethylhexanoate, toluene, 90 °C.

weights lower than targeted. We attribute these difficulties to interactions between the protected UPy comonomer and the copper catalyst. Increasing the concentration of the ligand (thereby decreasing the likelihood of copper–UPy interactions) marginally improved these polymerizations.

Given the difficulties associated with the aforementioned method, as well as our desire to probe the effect of varying

Scheme 2. Synthesis of UPy–Urethane Functionalized PMMAs via “Click” Chemistry^a



^a Reagents and conditions: (i) 12-azidododecan-1-ol, DBDTL, CH_2Cl_2 ; (ii) *o*-nitrobenzyl chloride, K_2CO_3 , DMF; (iii) $\text{Cu}(0)$, PMDETA, DMSO; (iv) TBAF, acetic acid, THF; (v) toluene, 95 °C (**6a** and **6b**) or THF, $\text{Cu}(0)$, PMDETA, 35 °C (**6c**).

UPy content on several polymers having identical contour length and size distribution, we sought a more efficient synthetic strategy. Synthesizing an alkyne functionalized PMMA and “clicking” the UPy–urethane moiety to the polymer proved a more effective route (Scheme 2). In addition to these general synthetic benefits, this method provides a reactive handle to further functionalize these particles for broader applicability.

In this synthesis we employed SET-LRP,⁴¹ both for the convenience of working with $\text{Cu}(0)$ when targeting higher molecular weights on a small scale and the reported accelerated polymerization times. Reacting **4** with clickable PMMA **5** afforded the protected, UPy functionalized precursor polymers **6** via thermal (**6a** and **6b**) or Cu mediated (**6c**) “click” reaction.⁴² In the case of the highest UPy–urethane loading Cu was needed to ensure complete conversion within a reasonable time frame (less than 72 h). These polymers are soluble in a wide range of organic solvents including THF, toluene, chloroform, and acetone. Hexanes and heptanes proved suitable for precipitation. The functionalized polymers have been characterized using all of the routine techniques; all spectra are in accordance with the assigned structures. GPC data are shown in Table 1.

Nanoparticle Fabrication and GPC Characterization. Nanoparticles are fabricated by dissolving the protected polymer in CHCl_3 (1 mg/mL) and irradiating with 350 nm UV light for 2 h (this is sufficient for complete deprotection by NMR based on our previous studies¹⁶). Consistent with previous covalently cross-linked SCNP work,^{7,8,11} the polymers show decreased hydrodynamic volume after deprotection, which relates to supramolecular cross-linker density (Table 1). This change in volume is a result of UPy dimerization after the

Table 1. Molecular Weight for Protected Polymers and Intramolecular Collapse

polymer	before irradiation		after irradiation for 1 h			after irradiation for 2 h		
	M_w^a (kg/mol)	M_w/M_n	M_w^a (kg/mol)	M_w/M_n	% change	M_w^a (kg/mol)	M_w/M_n	% change
2a → 3a	22.4	1.29	18.6	1.24	16	17.4	1.24	22
2b → 3b	18.5	1.39	15.9	1.40	14	14.9	1.40	19
6a → 7a	87.9	1.54	74.1	1.39	15	71.8	1.42	18
6b → 7b	82.0	1.4	69.2	1.38	16	62.0	1.32	24
6c → 7c	79.0	1.42	55.3	1.37	30	36.0	1.31	54
5	64.4	1.37				64.3	1.37	

^a Determined by GPC in THF versus PMMA standards.

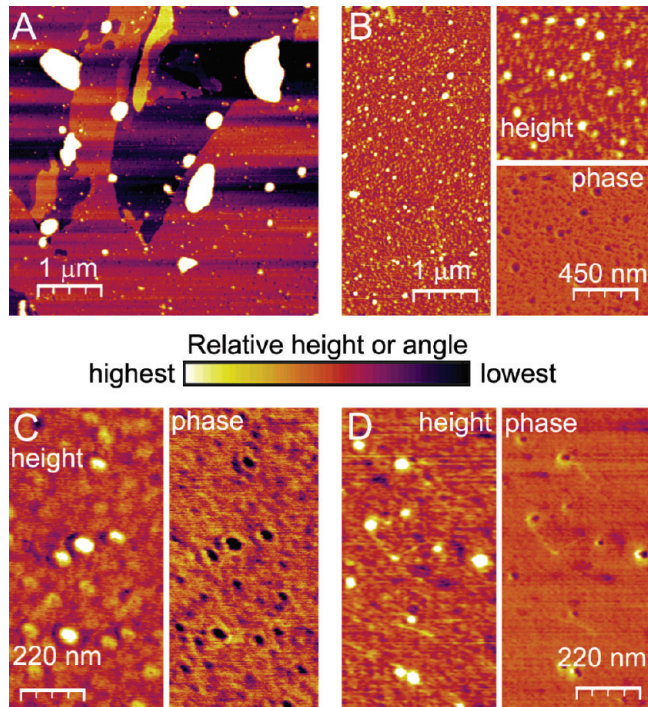


Figure 2. Supramolecular cross-linking monitored by AFM. All images were taken from samples of polymer **2b** (intermittently during conversion to **3b**) drop-cast ($2\mu\text{L}$ of a 10^{-8} mg/mL solution) on freshly cleaved mica. Panel A: protected polymer; panel B: following 30 min of irradiation (scale bar common for height and phase insets); panel C: following 60 min of irradiation; panel D: following 90 min of irradiation (scale bars are common in (C) and (D) for both height and phase panels).

release of the protecting group and subsequent collapse of the chain. Photodegradation of the backbone over this period can be ruled out as (1) the PDI does not increase after irradiation, as it would if chain scission were occurring, and (2) the UPy-free polymer **5** remains unchanged when exposed to deprotection conditions. Interestingly, when comparing the data for the protected polymers **6a**, **6b**, and **6c**, the polymers show a decrease in molecular weight with increasing protected UPy–urethane content. Despite the fact that the protected UPy groups are prevented from quadruple hydrogen bonding, drastically lowering the association constant, there still remain several available hydrogen-bonding sites. This results in the decreased hydrodynamic volume witnessed by GPC as the mole fraction of protected UPy–urethane in the polymer increases.

Deprotection Monitored by AFM. Consistent with the GPC results discussed above, the chain collapse process can be followed by AFM. Figure 2 shows that drop-casting protected polymer **2b** results in ill-defined clumps of polymer, occasionally with the presence of a few small spheres. The presence of these small particles even in the protected samples is not surprising considering that the protected UPy

and urethane groups still present several hydrogen-bonding sites available for supramolecular cross-linking, albeit with a significantly depressed association constant. Taking this into consideration, it may be the case that these weaker noncovalent interactions in essence prime the polymer for collapse and that the collapse itself resembles a cooperative process, proceeding quickly once the deprotection begins. AFM studies of the deprotection support this: after just 30 min of irradiation time, much shorter than what is required for complete deprotection by NMR, well-defined single particles are already present, and the ill-defined globs seen in the protected sample disappear. Visualization after 60 and 90 min of irradiation reveals that as deprotection time increases, particle size decreases: from $\sim 100\text{ nm}$ in diameter after 30 min to $\sim 75\text{ nm}$ in diameter after 60 min and $\sim 50\text{ nm}$ in diameter after 90 min. This is consistent with the GPC results as well as the aforementioned supramolecular cross-linking density dependence of particle size (increased irradiation time frees more UPy's for dimerization, thus increasing the density of supramolecular cross-links). Initial experiments on polymer samples lacking the urethane linker do not show the same behavior, again implying that the collapse relies on this secondary interaction between UPy–urethane dimers and in this way resembles the cooperative folding process witnessed in biomacromolecules.

AFM Characterization of Single-Chain Particles and Their Assemblies. Although fabrication of SCNP's is relatively simple, visualization of individual particles by AFM requires a bit of finesse to find the ideal conditions. Sample concentration and choice of surface and solvent strongly affect the data. Further, the polymer sample itself determines these conditions, as we have seen slight differences between these PMMA SCNP's and our previous PNB examples. If conditions are not perfect, aggregates of single particles dominate the images seen when conducting AFM characterization. This begs the question: how can one differentiate between these aggregates and individual nanoparticles? The following section explicitly describes this process.

Nanoparticles are first fabricated at 1 mg/mL , followed by serial dilutions for visualization (described in the experimental section). Trial and error is required to find an appropriate surface and solvent; for the samples discussed here the best results were obtained when solutions were drop-cast from chloroform onto a freshly cleaved mica surface. After selection of solvent and surface, measurements are conducted over a range of concentrations. While the actual concentrations required for visualizing each of the morphologies presented here depend on the polymer sample used, this method has been successfully applied to all of our SCNP examples.

Individual Single-Chain Particles. Drop-casting extremely dilute (10^{-8} – 10^{-10} mg/mL) nanoparticle solutions from CHCl_3 on mica results in large arrays of well-defined single-chain nanoparticles (Figure 3, panel A). We can be sure that the objects observed are single particles as dilution beyond this point results increasingly sparsely spaced particles of

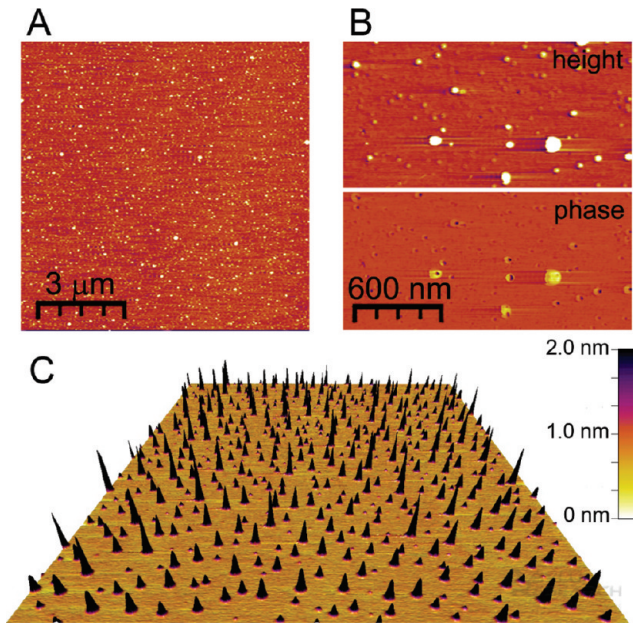


Figure 3. AFM images of single-chain particles drop cast ($2 \mu\text{L}$ of a 10^{-8} mg/mL solution) onto a mica surface: (A) $10 \times 10 \mu\text{m}$ scanning area displaying thousands of well-defined particles; (B) blown-up section of panel A and corresponding phase image showing the darkened core of individual particles; (C) $5 \times 5 \mu\text{m}$ scan shown in 3-D.

constant size. The size of these particles on the surface (see below) agrees well with our previous work.¹⁶ The estimated spherical radii of the particles agree well with the estimated R_g for PMMA of the same contour length. There is some size distribution to these individual particles; this is attributed to the molecular weight distribution of the polymer sample. The difference between small aggregates and individual SCNP is evident when comparing height and phase images (panel B); the single particles show a darkened core, whereas aggregates of a few particles show no changes in phase. We attribute this to phase separation of the UPy–urethane dimers from the PMMA backbone in the core of the particle.

Evidence for this internal organization of UPy–urethane dimers is observed via AFM when concentration is decreased to $\sim 10^{-12} \text{ mg/mL}$. While the particles appear to be flattened spheres or ellipsoids in the larger scans, high-resolution images of single particles reveal otherwise. Scanning an individual SCNP at high resolution reveals a complex geometry containing a raised center that is clearly visible in the height, phase, and amplitude images (Figure 4). The height of the central portion of the particle closely matches the size of the UPy–urethane dimer. This is consistent with the phase difference in the core of the particle as seen in the larger scans. In the high-resolution images this core is distinct from the rest of the particle in height and phase as well. This certainly supports the existence of a separate internal phase rich in UPy–urethane dimers. Whether or not the dimers are organized into well-ordered stacks is impossible to say for certain from this data; however, our efforts to better understand this behavior are continuous.

Table 2 summarizes the heights and diameters for each set of SCNP in this study as measured by AFM. As expected, the trends resemble that of analogous covalently cross-linked single chain particles: smaller particle size results from higher cross-link density, consistent with the GPC data. Comparing particles from polymer **3b** with **7a** shows an apparent (although not unexpected) molecular weight effect for

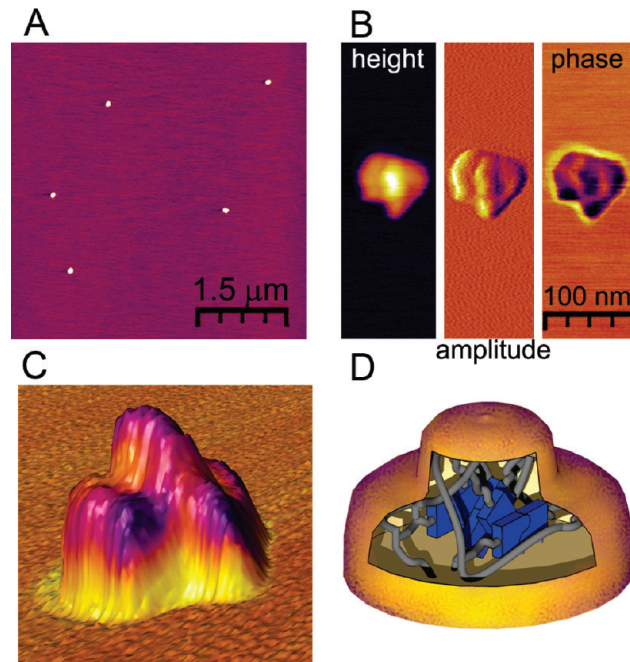


Figure 4. High-resolution AFM scan of individual SCNP: (A) group of a few particles; (B) height, amplitude, and phase images clearly indicating the complex geometry and raised core; (C) three-dimensional height image with phase retrace overlay of this particle. Panel D shows a cartoon depicting the possible particle morphology: UPy–urethane rich core (blue) immersed in a network of PMMA.

Table 2. Summary of Single Particle Sizes (in nm) by AFM

particle	height ^a	diameter ^a	estimated spherical radius ^b	estimated R_g ^c
3a	2–3	~35–50	10–12	12
3b	2–3	~35–50	10–12	11
7a	3–5	~100–200	30–35	22 ^d
7b	2–4	~100–150	20–25	22 ^d
7c	2–3	~50–75	12–20	22 ^d

^a From AFM images without tip correction (see Supporting Information for AFM height profiles). ^b Estimated by calculating the volume of the half-ellipsoid shaped particle on the surface and solving for the radius of a sphere (see Supporting Information). ^c Calculated using the formula $R_g = N^{0.6}$ where N is the estimated contour length of the polymer. ^d Calculated using the contour length of the clickable precursor polymer **5**.

polymers containing similar UPy–urethane concentration, although more detailed studies on the effect of molecular weight on particle size are underway. When comparing the sizes of the polymers to the estimated R_g , they may seem large for single chains: a collapsed particle, more like a hard sphere, would be smaller than the R_g in radius. There are, however, a few points that must be taken into consideration when discussing the estimates described here. First, the R_g estimates are very rough calculations based on the contour length of the clickable precursor and are only meant to provide some idea of dimensions for individual chains. Second, the diameters measured by AFM are artificially large due to the effects of the size and shape of the AFM tip. Third, the volume calculation assumes the particles on the surface resemble half-ellipsoid-like flattened spheres. This is an oversimplification, evident when viewing the single particle shown in Figure 3. The volume of the complicated “fried egg” geometry of the particles is likely overestimated by this calculation, leading to an overestimated spherical radius for the unflattened particle. Finally, the steric requirements for housing UPy–urethane dimers within a particle

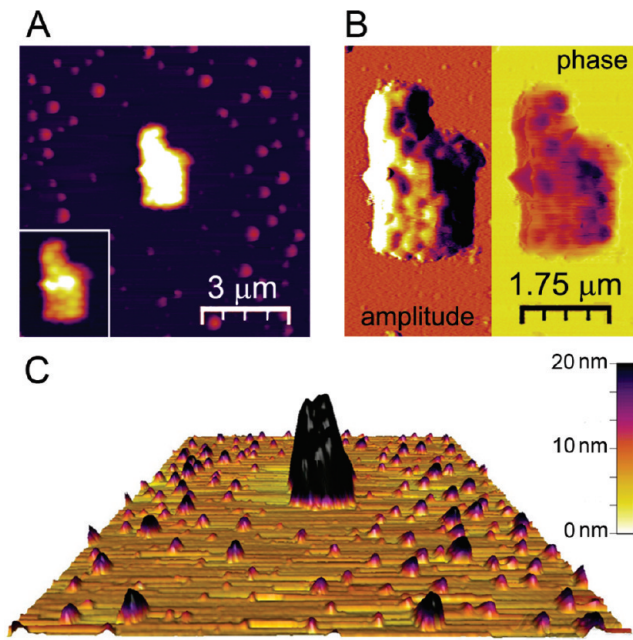


Figure 5. Aggregation of SCNP characterized by AFM: (A) large assembly of aggregates mediated by drying; (B) amplitude and phase images showing that this large assembly is comprised of smaller aggregates; (C) 3-D image of this large nanoparticle assembly.

are quite large, requiring a minimum interchain distance of roughly 6 nm. This means that there is a lower limit to how much collapse of the chain can actually occur, making a densely packed hard sphere an unlikely morphology for this system. When taking these points into consideration, the sizes witnessed here are perfectly reasonable for single chains.

Aggregates of Single-Chain Particles. Higher concentrations (10^{-6} – 10^{-7} mg/mL) results in larger disklike aggregates (~10 nm in height and a few hundred nanometers in diameter) along with even larger globules (Figure 5). These images again display nicely that this effect is a result of drying; the area immediately surrounding the large particle is void of smaller particles (panel A). In addition, the amplitude and phase images (panel B) show that this large object is indeed an assembly of smaller individual aggregates forced together by disappearing solvent, reminiscent of the “coffee stain” effect where the particles concentrate in the center of a drying drop during the final stages of solvent evaporation.^{43–45} This phenomenon is also known to create concentration gradients of deposited material on the surface, behavior we have also been able to visualize for our particles by AFM (see Supporting Information).

At concentrations in the range of 10^{-4} – 10^{-6} mg/mL large spherical agglomerates of particles appear (Figure 6). By filtering the sample through a 200 nm filter before drop-casting, we are certain that these large structures, on the order of several hundred nanometers up to a few micrometers in diameter and 20–50 nm high (panels A and B), are indeed the result of a drying effect. At concentrations in this range, another interesting phenomenon is witnessed: the appearance of tendril-like fibers, which are nucleated from the larger assemblies of particles seen in panel B (panels C and D). The height of these fibers is in agreement with the height of the SCNPs. In our last report we described this as linear assemblies of particles in which long stacks of dimerized UPy can extend beyond the individual particles creating these long fibers. This was witnessed previously only for the urea-containing polymers; the results here confirm that even with the decreased hydrogen-bonding ability of

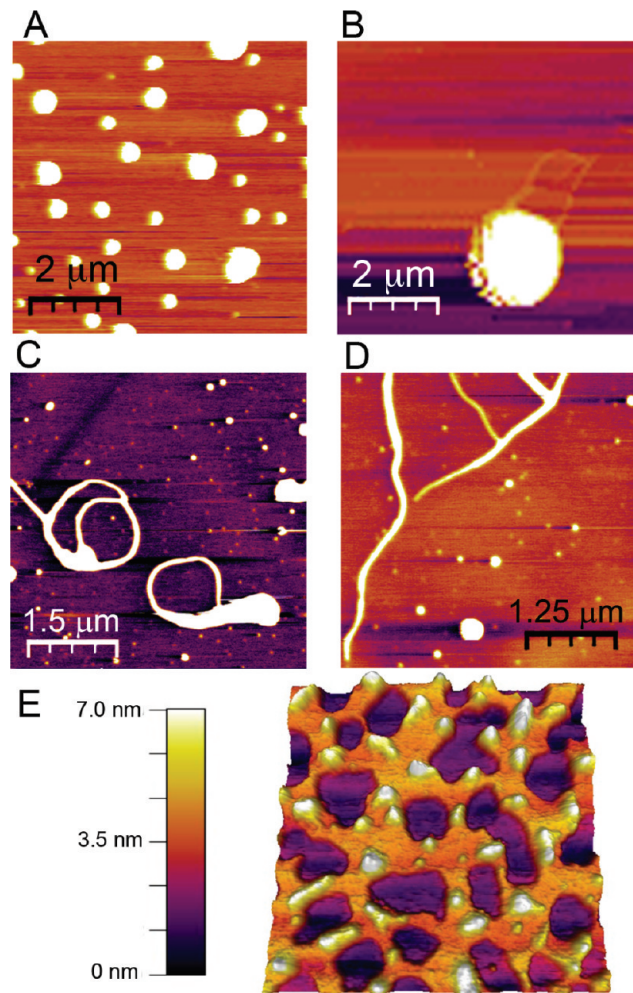


Figure 6. AFM image of large spherical aggregates, fibers, and networks of SCNPs: (A, B) large spherical aggregates; (C, D) fibers which appear nucleated from these larger assemblies; (E) $1 \times 1 \mu\text{m}$ scan of a network-like assembly of particles.

the UPy–urethane, there is still a significant driving force to create this type of assembly, possibly by some type of cooperative process. At the highest concentrations studied (typically from 1 to 0.001 mg/mL) network-like arrays of particles appear (panel E). This is in excellent agreement with comparative simulation and experimental studies conducted on the drying mediated self-assembly of inorganic nanoparticles.⁴⁵

The propensity for aggregation displayed by these particles on surfaces is also witnessed in solution. We believe that some of the structures described above, such as the fibers, actually begin to form in solution: on standing a transient network is formed that can be disturbed by sonication, reverting the system to free, individual particles.

Thermal Behavior of Protected Precursor Polymers and Bulk Nanoparticle Films. In our last report¹⁶ we discussed one possible application of these SCNPs: a solution processable formulation that could be turned into a high-performance supramolecular material. The initial solubility studies on the films of PMMA SCNP family are consistent with results obtained for the PNB systems; i.e., cast films remain soluble until thermal treatment induces the formation of an insoluble supramolecular network. Thermal investigations on bulk SCNPs and precursor polymers by DSC confirm this conjecture (Figure 7). Trends can be seen based on the amount of UPy–urethane incorporation that are consistent

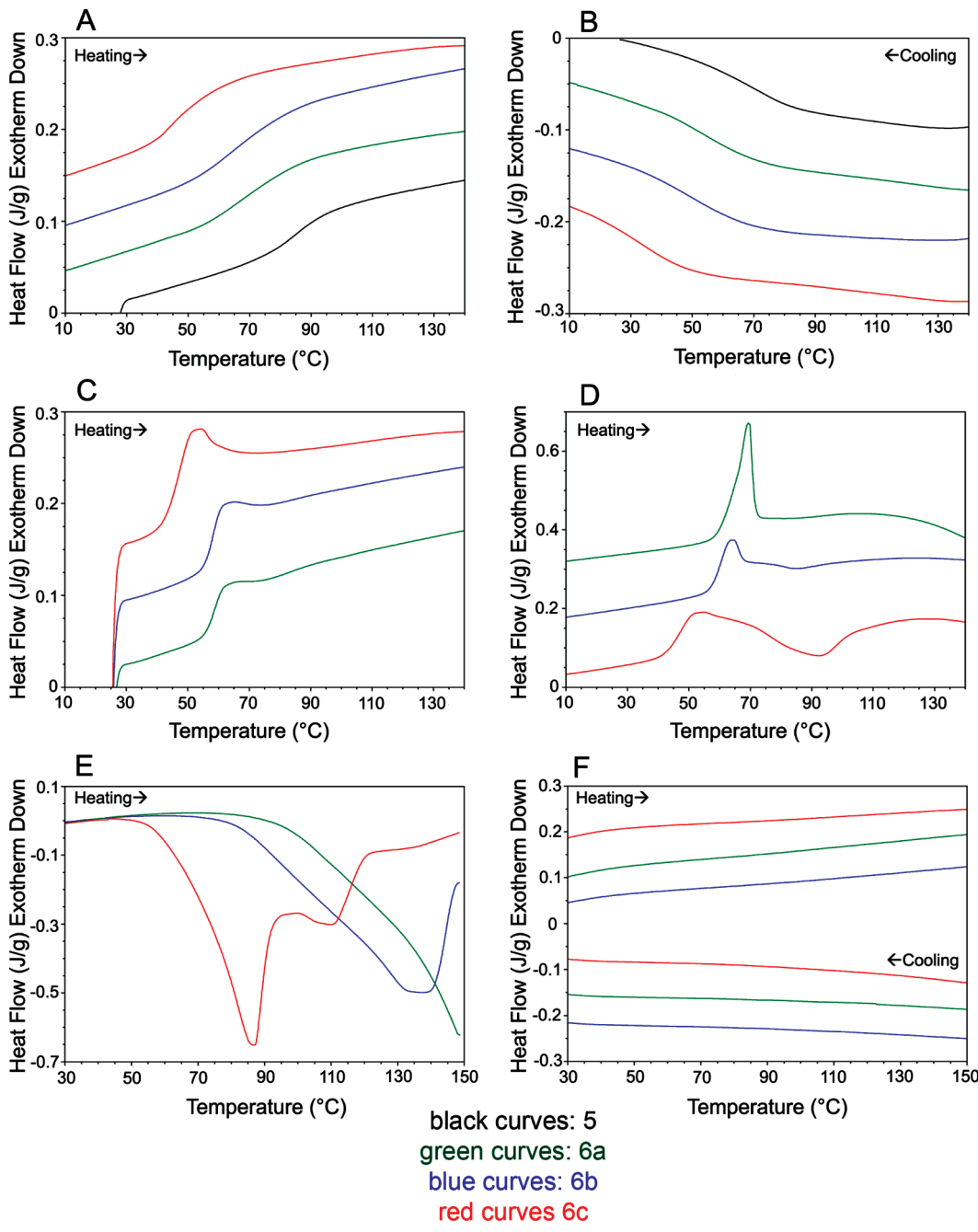


Figure 7. DSC data for protected polymers and SCNP film (arbitrary vertical offsets for clarity): (A) heating traces of protected polymers after erasure of thermal history; (B) cooling traces of protected polymers; (C) first heating traces for protected polymers after aging at room temperature for 48 h; (D) first heating traces for protected polymers after aging at room temperature for 1 week; (E) first heating trace of SCNP film; (F) subsequent heating and cooling traces of the SCNP film.

with trends witnessed in the AFM data discussed above. Panel A shows the heating traces for the protected polymers **6a**, **6b**, and **6c** as well as the “clickable” precursor **5**; panel B shows the corresponding cooling traces. Both cases reveal a decrease in T_g occurs with increasing UPy–urethane content. Looking at the first heating traces for the protected polymers after aging at room temperature displays the highly dynamic nature of this system. After just 48 h of aging (panel C) the heating traces show significant steepening of the T_g as well as shouldering due to enthalpic recovery. This is most pronounced with polymer **6c** having the highest amount of UPy–urethane incorporation and least so in **6a** with the least amount of UPy–urethane incorporation—not surprising as the increased density of hydrogen bonding sites will allow

faster reorganization of the material. The effects are more significant after 1 week of aging. Enthalpic events at T_g are now increasingly conspicuous, especially in sample **6a**. While this may seem incongruous with the previous result, examining the trace for **6c** reveals otherwise: a dynamic reorganization of the material occurs upon heating evident in the complex endothermic process that immediately follows T_g . Sample **6b**, with an intermediate amount of UPy–urethane content, displays behavior somewhere in between with a more detectable endothermic process than **6c** but a less decided exothermic process. The dynamic nature of the protected system demonstrated in these thermal experiments is in full agreement with the behavior witnessed during the AFM deprotection studies: in analogy to the intramolecular

hydrogen bonding that can prime the polymer in solution for collapse into a nanoparticle, aging the material results in enough hydrogen bonding to produce a morphology that is primed to reorganize once sufficient mobility is available after heating above T_g . This type of transient network formation has recently been characterized for UPy containing poly(butyl methacrylates);⁴⁶ similar to our results this behavior is strongly dependent on UPy content and distribution.

Thermal studies conducted on nanoparticle films confirm the applicability of this system to solution processable supramolecular materials. The first scan of the bulk SCNPs displays behavior completely different from the protected samples: unmistakable exothermic activity indicative of a curing process^{47–49} in which the nanoparticles unfold to form a network with intermolecular noncovalent cross-links. Once again, a trend can be seen based on the amount of UPy–urethane incorporation. In **6c** a distinct bimodal exotherm beginning just above T_g is seen. As UPy content decreases, this behavior becomes less distinct, with **6a** showing only broad exothermic activity beginning 30 °C above T_g and continuing over the entire temperature range, rather than the clear exotherm displayed by **6c**. This is not unexpected; with lower UPy–urethane density greater mobility (and therefore higher temperature) would be required to allow curing of material to occur via the reshuffling of UPy–urethane dimers (or monomers as would be the case at higher temperature). Once again, **6b** shows behavior in between the two extremes: a clear exothermic peak more similar to **6c**, but beginning nearly 30 °C above T_g (more similar to **6a**). All subsequent scans on all three samples reveal flat thermograms over the entire temperature range, confirming network formation upon thermal treatment. Decomposition of the UPy moieties can be ruled out as a cause for this change in behavior; in this case the polymer would still display a T_g for the unaffected PMMA portion. This is not witnessed in any of the heating or cooling traces for any of the cured nanoparticle samples, indicating that long-range motion in these samples is severely restricted by these supramolecular cross-links. Although the melting of well-ordered fibers in the cured samples was not witnessed, it does not rule out the likelihood of internal structure within the SCNP, as the formation of fibers long enough to produce a detectable thermal transition are unlikely within the nanoparticles and would be significantly hindered in the film by both the low mobility of the supramolecular network and the polarity of the PMMA matrix. Efforts are under way to scale up nanoparticle fabrication in order to produce gram or even kilogram quantities of these materials for exhaustive materials testing.

Summary

Our recently developed method for fabricating nanoparticles from single polymer chains has been expanded in both scope and utility in this report. We have introduced a new synthetic method for the facile production of protected UPy-decorated polymers that can be conjugated with further functionality, simultaneously demonstrating that this method is not only general but also tunable toward a number of applications. AFM experiments through serial dilution of nanoparticle samples display both the complex drying mediated self-assembly of these particles and confirm the identity of individual particles. The results of these studies indicate that through further development it may be possible to control this aggregation process and manipulate the self-organization of these structures into interesting and useful assemblies. Thorough AFM characterization of single particles has shown that they exhibit complex geometries that are likely

due to the existence of an internal phase rich in UPy–urethane dimers. AFM images taken at various stages of photodeprotection show that the polymers appear to be primed for rapid supramolecular collapse, resembling the cooperative process by which biomacromolecules fold. The applicability of this system to materials science has been demonstrated by thermal investigations: soluble films of nanoparticles undergo a curing process upon heating, reorganizing the material into an insoluble supramolecular network. While the behavior we described here is sophomore in comparison to the elegant natural structures from which we draw inspiration, we consider this an important advancement in controlling the way synthetic polymers can fold and self-assemble. Our efforts in this area continue, most specifically toward the development of catalytically active single-chain nanoparticles derived from complex architectures and diverse supramolecular cross-linking agents that can perform a more controlled collapse in an efficient and orthogonal fashion. In this way we hope to more closely mimic in synthetic systems the complex form and function of biomacromolecules.

Acknowledgment. The authors thank Dr. X. Lou, R. Bovee, and J. L. J. van Dongen for assistance with GPC characterization, A. J. H. Spiering for synthesis of some starting materials, and Dr. P. G. A. Janssen and Dr. P. E. L. G. Leclerc for enlightening discussions on AFM characterization. Additionally, the authors thank Prof. C. J. Hawker for his stimulating discussions and inspiration to enter the field of single-chain nanoparticles. The authors thank the Council for Chemical Sciences of The Netherlands Organization for Scientific Research (NWO-CW) for financial support as well as NSF DMR-05-20415 for travel support.

Supporting Information Available: Detailed experimental procedures, AFM images with height profiles, and full description for estimation of particle spherical radius. This material is available free of charge via the Internet at <http://pubs.acs.org>.

References and Notes

- (1) Sun, G.; Hagooly, A.; Xu, J.; Nyström, A. M.; Li, Z.; Rossin, R.; Moore, D. A.; Wooley, K. L.; Welch, M. J. *Biomacromolecules* **2008**, *9* (7), 1997–2006.
- (2) Seo, M.; Beck, B. J.; Paulusse, J. M. J.; Hawker, C. J.; Kim, S. Y. *Macromolecules* **2008**, *41* (17), 6413–6418.
- (3) Matson, J. B.; Grubbs, R. H. *J. Am. Chem. Soc.* **2008**, *130* (21), 6731–6733.
- (4) Luzuriaga, A. R. d.; Ormategui, N.; Grande, H. J.; Odriozola, I.; Pomposo, J. A.; Loinaz, I. *Macromol. Rapid Commun.* **2008**, *29* (12–13), 1156–1160.
- (5) Hales, K.; Chen, Z.; Wooley, K. L.; Pochan, D. J. *Nano Lett.* **2008**, *8* (7), 2023–2026.
- (6) Cheng, L.; Hou, G.; Miao, J.; Chen, D.; Jiang, M.; Zhu, L. *Macromolecules* **2008**, *41* (21), 8159–8166.
- (7) Croce, T. A.; Hamilton, S. K.; Chen, M. L.; Muchalski, H.; Harth, E. *Macromolecules* **2007**, *40* (17), 6028–6031.
- (8) Cherian, A. E.; Sun, F. C.; Sheiko, S. S.; Coates, G. W. *J. Am. Chem. Soc.* **2007**, *129* (37), 11350–11351.
- (9) Bertin, P. A.; Gibbs, J. M.; Shen, C. K.-F.; Thaxton, C. S.; Russin, W. A.; Mirkin, C. A.; Nguyen, S. T. *J. Am. Chem. Soc.* **2006**, *128* (13), 4168–4169.
- (10) Hawker, C. J.; Wooley, K. L. *Science* **2005**, *309* (5738), 1200–1205.
- (11) Harth, E.; Horn, B. V.; Lee, V. Y.; Germack, D. S.; Gonzales, C. P.; Miller, R. D.; Hawker, C. J. *J. Am. Chem. Soc.* **2002**, *124* (29), 8653–8660.
- (12) Rodriguez-Hernandez, J.; Checot, F.; Gnanou, Y.; Lecommandoux, S. *Prog. Polym. Sci.* **2005**, *30* (7), 691–724.
- (13) Pochan, D. J.; Chen, Z.; Cui, H.; Hales, K.; Qi, K.; Wooley, K. L. *Science* **2004**, *306* (5693), 94–97.
- (14) Nyström, A. M.; Bartels, J. W.; Du, W.; Wooley, K. L. *J. Polym. Sci., Part A: Polym. Chem.* **2009**, *47* (4), 1023–1037.
- (15) Hamilton, S. K.; Harth, E. *ACS Nano* **2009**, *3* (2), 402–410.
- (16) Foster, E. J.; Berda, E. B.; Meijer, E. W. *J. Am. Chem. Soc.* **2009**, *131* (20), 6964–6966.

- (17) Beck, J. B.; Killops, K. L.; Kang, T.; Sivanandan, K.; Bayles, A.; Mackay, M. E.; Wooley, K. L.; Hawker, C. J. *Macromolecules* **2009**, *42* (15), 5629–5635.
- (18) Adkins, C. T.; Muchalski, H.; Harth, E. *Macromolecules* **2009**.
- (19) Hill, D. J.; Mio, M. J.; Prince, R. B.; Hughes, T. S.; Moore, J. S. *Chem. Rev.* **2001**, *101* (12), 3893–4012.
- (20) Walker, R.; Conrad, R. M.; Grubbs, R. H. *Macromolecules* **2009**, *42* (3), 599–605.
- (21) Stubenrauch, K.; Gerhard, I. V.; Fritz-Popovski; Trimmel, G. *J. Polym. Sci., Part A: Polym. Chem.* **2009**, *47* (4), 1178–1191.
- (22) Matson, J. B.; Virgil, S. C.; Grubbs, R. H. *J. Am. Chem. Soc.* **2009**, *131* (9), 3355–3362.
- (23) Lienkamp, K.; Kins, C. F.; Alfred, S. F.; Madkour, A. E.; Tew, G. N. *J. Polym. Sci., Part A: Polym. Chem.* **2009**, *47* (5), 1266–1273.
- (24) Matson, J. B.; Grubbs, R. H. *Macromolecules* **2008**, *41* (15), 5626–5631.
- (25) Dong, H.; Matyjaszewski, K. *Macromolecules* **2008**, *41* (19), 6868–6870.
- (26) Mueller, L.; Jakubowski, W.; Tang, W.; Matyjaszewski, K. *Macromolecules* **2007**, *40* (18), 6464–6472.
- (27) Min, K.; Gao, H.; Matyjaszewski, K. *Macromolecules* **2007**, *40* (6), 1789–1791.
- (28) Matyjaszewski, K.; Tsarevsky, N. V.; Braunecker, W. A.; Dong, H.; Huang, J.; Jakubowski, W.; Kwak, Y.; Nicolay, R.; Tang, W.; Yoon, J. A. *Macromolecules* **2007**, *40* (22), 7795–7806.
- (29) Teoh, R. L.; Guice, K. B.; Loo, Y.-L. *Macromolecules* **2006**, *39* (25), 8609–8615.
- (30) Ladmiral, V.; Mantovani, G.; Clarkson, G. J.; Cauet, S.; Irwin, J. L.; Haddleton, D. M. *J. Am. Chem. Soc.* **2006**, *128* (14), 4823–4830.
- (31) Jakubowski, W.; Min, K.; Matyjaszewski, K. *Macromolecules* **2006**, *39* (1), 39–45.
- (32) Jakubowski, W.; Matyjaszewski, K. *Angew. Chem., Int. Ed.* **2006**, *45* (27), 4482–4486.
- (33) Matyjaszewski, K.; Xia, J. *Chem. Rev.* **2001**, *101* (9), 2921–2990.
- (34) Nguyen, N. H.; Rosen, B. M.; Lligadas, G.; Percec, V. *Macromolecules* **2009**, *42* (7), 2379–2386.
- (35) Wright, P. M.; Mantovani, G.; Haddleton, D. M. *J. Polym. Sci., Part A: Polym. Chem.* **2008**, *46* (22), 7376–7385.
- (36) Lligadas, G.; Rosen, B. M.; Bell, C. A.; Monteiro, M. J.; Percec, V. *Macromolecules* **2008**, *41* (22), 8365–8371.
- (37) Lligadas, G.; Percec, V. *J. Polym. Sci., Part A: Polym. Chem.* **2008**, *46* (10), 3174–3181.
- (38) Lligadas, G.; Percec, V. *J. Polym. Sci., Part A: Polym. Chem.* **2008**, *46* (8), 2745–2754.
- (39) Gerard Lligadas, V. *P. J. Polym. Sci., Part A: Polym. Chem.* **2008**, *46* (20), 6880–6895.
- (40) Rosen, B. M.; Percec, V. *J. Polym. Sci., Part A: Polym. Chem.* **2007**, *45* (21), 4950–4964.
- (41) Percec, V.; Guliashvili, T.; Ladislaw, J. S.; Wistrand, A.; Stjerndahl, A.; Sienkowska, M. J.; Monteiro, M. J.; Sahoo, S. *J. Am. Chem. Soc.* **2006**, *128* (43), 14156–14165.
- (42) Bräse, S.; Gil, C.; Knepper, K.; Zimmermann, V. *Angew. Chem., Int. Ed.* **2005**, *44* (33), 5188–5240.
- (43) Hu, H.; Larson, R. G. *J. Phys. Chem. B* **2006**, *110* (14), 7090–7094.
- (44) Kajiyama, T.; Kaneko, D.; Doi, M. *Langmuir* **2008**, *24* (21), 12369–12374.
- (45) Rabani, E.; Reichman, D. R.; Geissler, P. L.; Brus, L. E. *Nature* **2003**, *426* (6964), 271–274.
- (46) Feldman, K. E.; Kade, M. J.; Meijer, E. W.; Hawker, C. J.; Kramer, E. J. *Macromolecules* **2009**, ASAP.
- (47) Tripathi, G.; Srivastava, D. *J. Appl. Polym. Sci.* **2009**, *112* (5), 3119–3126.
- (48) Darshan; Malhotra, P.; Narula, A. K. *J. Appl. Polym. Sci.* **2009**, *113* (1), 216–225.
- (49) Ai, H.; Xu, K.; Liu, H.; Chen, M.; Zhang, X. *J. Appl. Polym. Sci.* **2009**, *113* (1), 541–546.